Zero-velocity atom interferometry using a retroreflected frequency-chirped laser

I. Perrin, J. Bernard, Y. Bidel, A. Bonnin, N. Zahzam, C. Blanchard, and A. Bresson
DPHY, ONERA, Université Paris Saclay, F-91123 Palaiseau, France

M. Cadoret*
LCM-CNAM, 61 rue du Landy, 93210, La Plaine Saint-Denis, France

(Received 8 July 2019; published 21 November 2019)

Atom interferometry using stimulated Raman transitions in a retroreflected configuration is the first choice in high-precision measurements because it provides low phase noise, a high-quality Raman wave front, and a simple experimental setup. However, it cannot be used for atoms at zero velocity because two pairs of Raman lasers are simultaneously resonant. Here we report a method which allows this degeneracy to be lifted by using a frequency chirp on the Raman lasers. Using this technique, we realize a Mach-Zehnder atom interferometer hybridized with a force balanced accelerometer which provides horizontal acceleration measurements with a short-term sensitivity of $3.2 \times 10^{-5}\ \mathrm{m\,s^{-2}}/\sqrt{\mathrm{Hz}}$. This technique could be used for multiaxis inertial sensors, tiltmeters, or atom interferometry in a microgravity environment.

DOI: 10.1103/PhysRevA.100.053618

I. INTRODUCTION

Since their inception, light-pulse atom interferometers (AIs) have proven to be extremely sensitive gravito-inertial sensors measuring gravity [1–5], gravity gradients [6–8], and rotations [9–12], appearing as promising candidates to compete with traditional sensors used for geodesy, geophysics, exploration, or inertial navigation [13]. Moreover, they have proved to be an invaluable tool in fundamental physics, where they are used for measuring physical constants [14–17], testing the Einstein equivalence principle [18–22], searching for dark sector particles [23], and have even been proposed for gravitational-wave detection [24,25] or for measuring free fall of antimatter [26]. The principle of a light-pulse AI relies on the use of recoils from photon-atom interactions to coherently split, deflect, and interfere matter waves. Most light-pulse AIs use a stimulated two-photon process (Raman or Bragg transitions) to realize the beamsplitters and mirrors required for the interferometer sequence [27]. In this process, the atom coherently absorbs and then emits a photon from a pair of counterpropagating laser beams with different frequencies, resulting in a net momentum transfer of $\hbar k_{\mathrm{eff}}$ at each interaction, where k_{eff} is the effective wave vector. To perform Bragg-based or Raman-based AIs at their best level of performance, it is beneficial to address the two-photon transitions in a retroreflected geometry where a single laser beam with two laser frequencies is retroreflected off a mirror. First, this allows a reduction of the effect of wave-front distortions which affect the sensor's accuracy [28]. This is because the wave-front distortion of the incoming beam cancels out in a retroreflected configuration and only optical elements behind the atoms have to be considered for wave-front distortions (mirror, wave plate, vacuum window). Second, it is an efficient way to implement the k_{eff} reversal technique [29] to eliminate some systematics, as well as to reduce interferometer phase noise, as most vibration effects on the laser phases are common to the two lasers and cancel out in the two-photon process, apart from vibrations of the mirror. However, the use of retroreflection for zero-velocity atoms along the Raman beam naturally leads to a double diffraction scheme where two stimulated Raman transitions with opposite momentum transfer $\pm\hbar k_{\mathrm{eff}}$ are simultaneously resonant. This double diffraction scheme has been first implemented using Raman transitions to realize an AI for which the separation between the two arms is $2\hbar k_{\mathrm{eff}}$, both in the case of atoms at rest [30], as well as for nonvanishing initial velocities in the case of a gravimeter [31]. For the latter, three laser frequencies were mandatory to account for the changing Doppler shift induced by gravity acceleration, hence leading to a more complex setup. However, for onboard applications, where shot-to-shot acceleration variations leads to uncontrolled velocity variations of the atomic sample, even though close to zero velocity, it becomes challenging to address this double diffraction scheme with high efficiency, as the two transitions become partly degenerated. Moreover, the experimental realization of a double-diffraction AI geometry is much more demanding than that of a single diffraction, as it requires a longer Raman pulse duration, colder atomic source, and additional blow-away beams to get rid of parasitic interferometers. In addition, the gain in scale factor obtained by increasing the arm separation in a double diffraction scheme is not of interest when the sensitivity of the interferometer is limited by vibrations unless used in a differential mode accelerometer for applications in gradiometry [32] or for testing the weak equivalence principle [22]. Therefore, in certain situations, single diffraction may be preferable to double diffraction. In this work, we experimentally demonstrate a technique enabling

*malo.cadoret@lecnam.net

the use of single-diffraction two-photon Raman transitions despite a zero Doppler shift in the commonly used retroreflected geometry. By employing a laser frequency chirp, we lift the degeneracy between the two simultaneous resonance transitions. We then apply our technique to the measurement of the horizontal component of acceleration using a Mach-Zehnder–style atom interferometer. We achieve a sensitivity of 3.2×10^{-5} m s$^{-2}/\sqrt{\text{Hz}}$ and show that no bias is induced by this method.

II. METHOD

We present here a general method which can be applied to any two-photon process such as Raman transition or Bragg diffraction. For example, we demonstrate our technique by performing stimulated two-photon Raman transitions between the two hyperfine ground states of ^{87}Rb (labeled $|g\rangle$ and $|e\rangle$) via an intermediate state (labeled $|i\rangle$) using two lasers of frequencies ω_1 and ω_2 detuned to the red of the D_2 line by Δ_i. The Raman beams are brought to the vacuum chamber via a polarization-maintaining optical fiber. After passing through the chamber, the laser beams are retroreflected through a quarter-wave plate to rotate the initial polarization into its orthogonal polarization, creating two pairs of counterpropagating beams in the horizontal x direction in a lin $\perp$ lin configuration [see Fig. 1(a)]. Consequently, two pairs of beams can drive the two-photon transition between $|F = 1, m_F = 0\rangle \equiv |g\rangle \rightarrow |F = 2, m_F = 0\rangle \equiv |e\rangle$. With this polarization configuration, the copropagating Raman transitions are forbidden. The detuning δ from the two-photon resonance is given by

$$\delta = \omega_1 - \omega_2 - (\omega_0 + \omega_D + \omega_R), \tag{1}$$

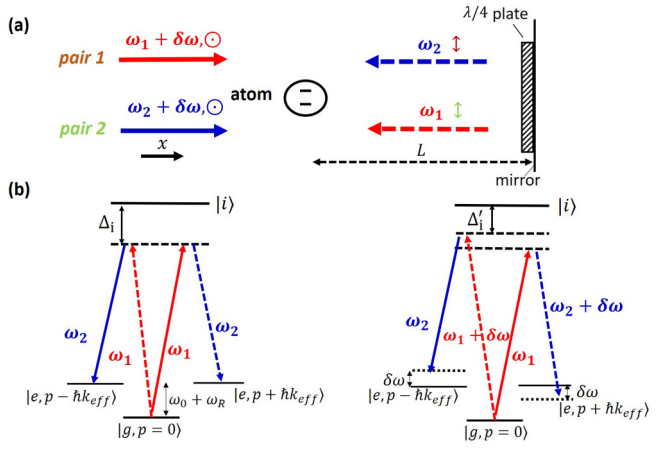

FIG. 1. (a) Schematic setup of two-photon Raman transitions in the commonly used retroreflecting geometry. A two-level atom is interacting with two pairs of counterpropagating light fields (pair 1 and pair 2) in lin $\perp$ lin configuration. Applying a frequency chirp β on the lasers changes the incident laser frequency by $\delta\omega = 2\pi\beta t_d$. Δ_i is the one-photon detuning. (b) Left: Scheme of the Raman transition between the two hyperfine ground states of an alkaline atom in the absence of Doppler shift ($\omega_D = 0$) and without frequency chirp ($\beta = 0$). Both pairs are simultaneously resonant. Right: Applying a frequency chirp β on the Raman laser frequencies lifts the degeneracy between the two resonant conditions by an amount $2\delta\omega$. After the chirp, the one-photon detuning is Δ_i'.

where ω_0 is the frequency of the hyperfine transition, $\omega_D = \pm\vec{k}_{\text{eff}} \cdot \vec{v}$ is the Doppler shift due to the atomic velocity $\vec{v}$ in the reference frame of the apparatus, and $\omega_R = \frac{\hbar k_{\text{eff}}^2}{2m}$ the recoil frequency shift. Thus, in the absence of Doppler shift, both pairs are simultaneously resonant and couple $|g, \vec{p}\rangle \rightarrow |e, \vec{p} \pm \hbar\vec{k}_{\text{eff}}\rangle$. In order to circumvent this problem and lift the degeneracy between the two resonance conditions, we apply a frequency chirp $\beta = \frac{1}{2\pi}\frac{d\omega_1}{dt} = \frac{1}{2\pi}\frac{d\omega_2}{dt}$ on the Raman lasers. As the reflected beams are delayed with respect to the incoming ones by $t_d = \frac{2L}{c}$ (where L is the atom-mirror distance), the incoming laser frequencies will be shifted by $\delta\omega = 2\pi\beta t_d$ at the position of the atoms, allowing one transition to be detuned with respect to the other by $2\delta\omega$. This allows one to selectively address Raman pair 1 or pair 2. This effect can be understood as mimicking an effective atomic velocity in the reference frame of the lasers, leading to an equivalent Doppler shift $\omega_D = 2\pi\beta t_d$.

A. Experimental setup and lasers

The experiment was carried out in the atom interferometer setup described in [33]. Atom interferometers usually consist of three steps: preparation, interferometry, and population detection. To perform these functions we use the laser system described in detail in [34] based on a frequency-doubled fiber bench using two independent lasers sharing the same 5 W erbium-doped fiber amplifier (EDFA). The laser used to cool and detect the atoms is an erbium distributed feedback (DFB) fiber laser at 1.5 μm (output power 20 mW, linewidth 2 kHz) locked relative to the rubidium transitions using a saturated absorption lock [35]. The AI laser source is a DFB laser diode at 1.5 μm (output power 10 mW, linewidth 1 MHz). The detuning Δ of the AI laser from the one-photon resonance is controlled using a beat note between the two lasers at 1.5 μm. Finally the two lasers are combined at 1.5 μm by an electro-optical modulator which acts like a continuous optical switch between each laser before seeding the EDFA. The output of the EDFA is sent to the dual-wavelength second harmonic generation bench. In our experiment, the two Raman beam frequencies are generated thanks to a fiber phase modulator [36]. The chirp β is obtained by directly modulating the input current of the laser diode using a low-frequency arbitrary wave-form generator (AWG). We display in Fig. 2 the laser setup and the optical bench of the experiment.

B. Raman spectroscopy experiment

To investigate our method, we first started by implementing Raman spectroscopy. A cold ^{87}Rb atom sample is produced in a three-dimensional magneto-optical trap (MOT) loaded from a background vapor pressure in 340 ms. Atoms are further cooled to 2 μK by means of a polarization gradient in 8 ms. The cooling beams are then turned off, and as the atoms freely fall, a microwave π pulse followed by a blow-away beam allows one to select the atoms in the insensitive ground state $|F = 1, m_F = 0\rangle$ with a horizontal bias magnetic field of 100 mG. Then, a horizontal Raman laser pulse of duration $\tau = 10$ μs is applied to the atoms 18 ms after their release from the trap. The proportion of atoms in each hyperfine state $F = 1$ and $F = 2$ is then measured using a state-selective

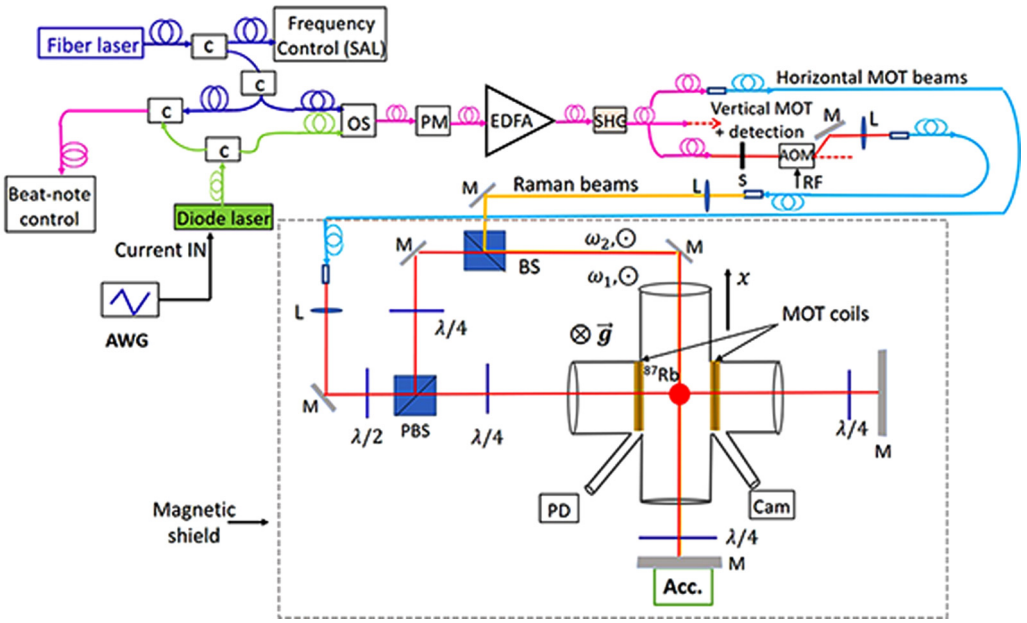

FIG. 2. Scheme of the laser system and the experimental setup (top view) allowing Raman transitions to be performed in the horizontal scheme: SAL, saturated absorption lock; L, lens; M, mirror; PM, phase modulator; AOM, acousto-optic modulator; S, shutter; PBS, polarizing beam-splitter; OS, optical switch; BS, beam splitter; AWG, arbitrary wave-form generator; SHG, second harmonic generation; Acc, accelerometer; c, coupler; PD, photodetector; Cam, camera.

vertical light-induced fluorescence detection. The cycling time of the experiment is $T_{\text{cycle}} = 500$ ms. In practice, the AWG generates a triangle-wave modulation signal in burst mode, directly applied to the modulation input of the laser diode current controller. The voltage command signal is triggered to the Raman pulse, and the chirp duration is fixed to 40 μs. Consequently, the single-photon frequency excursion is controlled by adjusting the peak-to-peak voltage amplitude denoted A. We experimentally measure the frequency response of the laser diode as a function of the voltage amplitude by monitoring the beat-note signal between the laser diode and the fiber laser using the fast Fourier transform (FFT) math function of an oscilloscope. Figure 3 displays the frequency response of the laser diode when applying $A = 6$ V peak-to-peak amplitude command. For clarity sake, the frequency response is plotted as the frequency difference between the Raman laser frequency $\nu_{\text{Raman}} = \omega_1/2\pi$ and the $5S_{1/2}, F = 2 \rightarrow 5P_{3/2}, F' = 1$ transition. In this case, one finds a chirp $\beta = -210$ MHz μs^{-1}. The delay between the command and the Raman laser pulse is adjusted to ensure a linear frequency response of the laser diode during the Raman pulse.

Figure 4 displays the measured transition probability as a function of the Raman frequency difference $(\omega_1 - \omega_2)/2\pi$ for different chirp values β applied to the laser diode. The Raman laser intensity is adjusted to maximize the transfer efficiency at resonance for a pulse duration of $\tau = 10$ μs. When no chirp is applied ($\beta = 0$), only a single peak is observed due to the simultaneous resonant condition. Increasing β slightly starts lifting the degeneracy between the two resonant conditions. For $\beta = -35$ MHz μs^{-1}, the chirp is not important enough to lift the degeneracy between the two transitions. However, for greater values of the chirp, two resonance spectra are clearly observed with a frequency separation which increases linearly with the amplitude of the voltage command. Measuring the frequency separation between the two resonance spectra $(2\delta\omega/2\pi)$ allows one to estimate the atom-mirror distance $L = c\delta\omega/4\pi\beta \simeq 24$ cm, in agreement with the expected distance from the trap center to the mirror of the setup.

III. ATOM INTERFEROMETER

To further investigate our technique we performed a Mach-Zehnder–style AI in a horizontal configuration using a $\pi/2 - \pi - \pi/2$ chirped Raman pulse sequence, with each pulse separated by an interrogation time T. With this geometry,

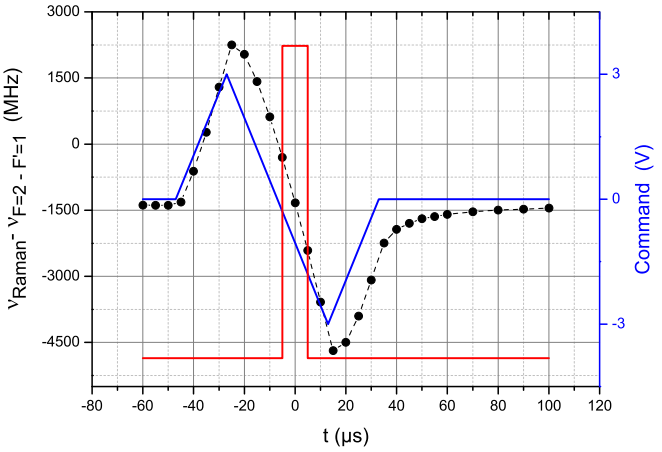

FIG. 3. Frequency response of the Raman laser $\nu_{\text{Raman}} = \frac{\omega_1}{2\pi}$ to the voltage command applied to the current modulation input. Voltage command (blue line). Measurement of the laser diode frequency response (black dots and line). Raman laser pulse (red line). The measured chirp is $\beta = -210$ MHz μs^{-1}, leading to a frequency excursion of 2100 MHz during the Raman pulse.

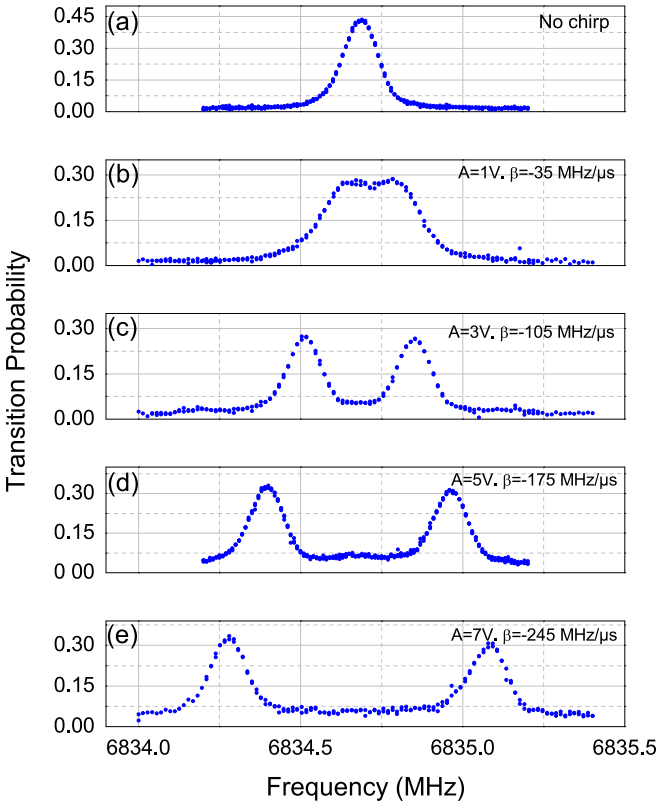

FIG. 4. Raman resonance spectra obtained by scanning the Raman frequency difference $(\omega_1 - \omega_2)/2\pi$ across the resonance for five different frequency chirps applied on the laser diode. A is the peak-to-peak amplitude voltage of the signal command. (a) For $\beta = 0$ a single peak is observed due to the simultaneous resonant conditions. (b)–(e) When applying a frequency chirp two peaks are observed allowing the degeneracy between the two Raman transitions to be lifted. The two Raman resonances are separated by $2\delta\omega/2\pi$.

the atomic phase shift at the output of the interferometer is sensitive to the horizontal acceleration $\vec{a}$ of the atoms relative to the reference mirror. In the limit of short, resonant pulses, the phase shift is then given by $\Delta\phi = \phi_1 - 2\phi_2 + \phi_3 = \vec{k}_{\text{eff}} \cdot \vec{a}\, T^2$, where ϕ_i is the phase difference between the two counterpropagating Raman lasers at the position of the atoms at the ith Raman pulse. The delay between the release of the atoms from the trap and the first Raman pulse is $t_0 = 3$ ms. The Raman beams have a waist of 5.5 mm ($1/e^2$ radius). Thus, due to the free fall of the atoms across the laser beam, our interrogation time is limited and the intensity seen by the atoms for the three laser pulses will be different. Consequently, we adjust the timing of our experiment and the position of the laser beam in order to have the same intensity seen by the atoms for the first and the last Raman pulses. This leads to an interrogation time $2T = 31.7$ ms. This configuration enables light-shift effects to be minimized. As the intensity is higher for the middle pulse (π), this configuration also allows the same pulse duration ($\tau = 10\ \mu$s) to be applied for the three Raman laser pulses without losing too much contrast.

Consequently, we ensure the frequency chirp to be the same for each Raman pulse, $\beta = -210$ MHz μs^{-1} in our experiment. Figure 5 is a sketch of the interferometer setup.

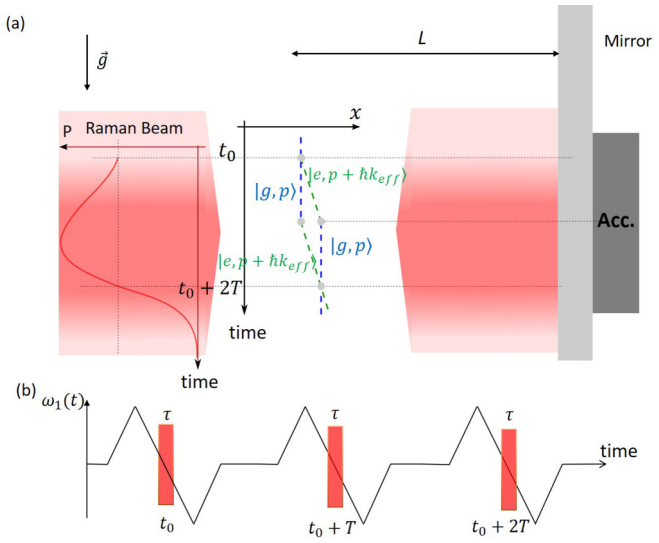

FIG. 5. (a) Sketch of the horizontal atomic accelerometer. The atoms fall under gravity in the retroreflected Raman beam. By measuring the transition probability P as a function of free-fall time of the atoms, we adjust the timing of our experiment and the position of the Raman laser beam. The pulse duration is equal for the three Raman light pulses. The center of the classical accelerometer (Acc.) matches the position of the cold atom cloud at the π pulse. $L = 24$ cm: atom-mirror distance. (b) Raman frequency $\omega_1(t)$ during the interferometer sequence. The same linear chirp is applied for the three Raman pulses.

After the interferometer sequence we measure the proportion of atoms in each output port of the AI by fluorescence. The normalized proportion of atoms in the hyperfine state $|F = 2, m_F = 0\rangle$ after the final $\pi/2$ pulse is a sinusoidal function of the acceleration:

$$P = P_m - \frac{C}{2}\cos(\vec{k}_{\text{eff}} \cdot \vec{a}\, T^2), \tag{2}$$

where P_m is the fringe offset and C the fringe contrast. In a retroreflected geometry, the phase is sensitive to the acceleration of the atom compared to the mirror. Thus, in absence of vibration isolation, fluctuations of the mirror position can induce fluctuations of the interferometer phase, which wash out the fringe visibility, even in the laboratory environment. To observe interference fringes, we perform a correlation-based technique [37] combining the simultaneous measurements of the output signal P of our interferometer with that from a classical accelerometer rigidly fixed to the Raman mirror. This allows the interference fringes to be recovered, although the fringes are randomly scanned by vibrations. Figure 6 displays retrieval of the fringe pattern obtained by plotting the probability transition of the AI output versus the acceleration measured by the classical accelerometer. The fringe contrast obtained from the sinusoidal least-squares fit of the data is $C = 40\%$.

In order to work at the best sensitivity, we studied the contrast of the interferometer as a function of the frequency chirp β applied on the Raman lasers. Results are displayed in Fig. 7. The contrast is an increasing function of the frequency chirp β until it reaches an optimum of $C = 40\%$ for

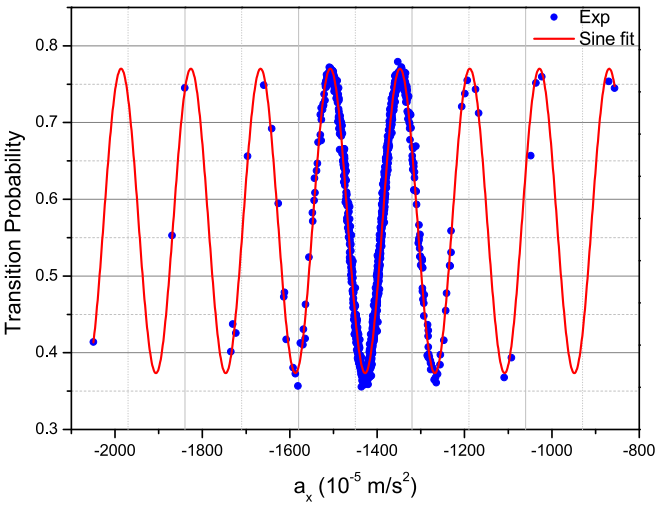

FIG. 6. Horizontal atom interferometer fringe pattern. The total interferometer time is $2T = 31.7$ ms, and the frequency chirp applied during each Raman pulse is set to $\beta = -210$ MHz μs^{-1}. The solid line is a sinusoidal least-squares fit using Eq. (2). The estimated fringe contrast is $C \sim 40\%$.

$\beta = -200$ MHz μs^{-1}. Increasing further the chirp value does not improve the interferometer's contrast.

A. Atom accelerometer sensitivity

To analyze the sensitivity and the stability of the horizontal atom accelerometer, we performed a hybridization of the classical accelerometer with the atom interferometer. We use the hybridization procedure described in [4]. We operated the atomic sensor continuously during one night. Figure 8 displays the Allan standard deviation (ADEV) of the hybridized atomic accelerometer signal. The sign of the effective Raman wave vector $\vec{k}_{\text{eff}}$ is reversed every measurement cycle. We achieve a short-term sensitivity of 3.2×10^{-5} m s$^{-2}/\sqrt{\text{Hz}}$, which is comparable to state of the art for horizontal configurations [38] (1×10^{-5} m s$^{-2}/\sqrt{\text{Hz}}$), despite the use of a shorter interrogation time (31.7 versus 226 ms). The ADEV of

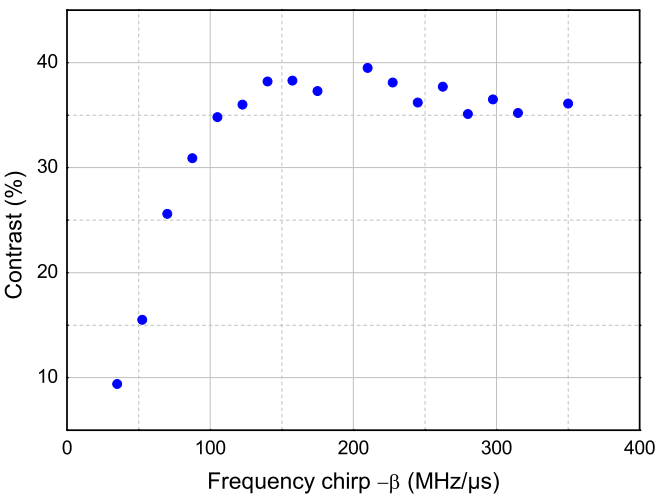

FIG. 7. Contrast as a function of the frequency chirp.

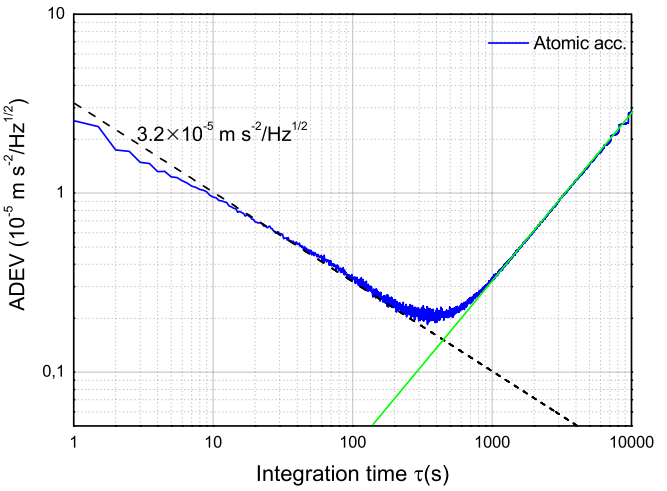

FIG. 8. Allan standard deviation (ADEV) of the atomic accelerometer (blue line). The dash line illustrates the $\tau^{-1/2}$ scaling. The green line illustrates the τ scaling.

the horizontal acceleration measurement scales as $\tau^{-1/2}$ and reaches 0.2×10^{-5} m s^{-2} at 500 s integration time. For longer integration times, the acceleration measurement drifts as illustrated by the typical linear dependence in the averaging time τ. The observed drift could be caused by an angular variation of the Raman mirror. The atom interferometer is measuring the projection of the gravity along the normal of the mirror. An angular drift of the mirror of 10 μrad, which seems reasonable in our experimental setup, could explain the observed drift. Thus, one cannot draw conclusions regarding the long-term stability of the atom accelerometer unless using an auxiliary tilt sensor to monitor the angle between the Raman beam and the horizontal plane during the measurement.

B. Bias arising from the frequency chirp

To conclude our study, we investigated a possible bias induced by the frequency chirp β on the acceleration

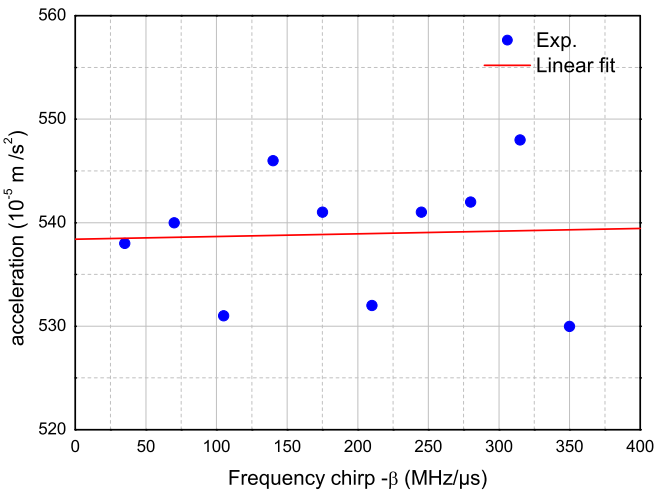

FIG. 9. Acceleration as a function of the chirp β applied on the Raman lasers. The line (in red) is a linear fit to the data points. The slope is $0.3 \pm 2 \times 10^{-7}$ m s^{-2}/MHz μs^{-1}.

measurement. The phase added by the frequency ramps adds a noninertial contribution to the atomic phase shift (see Appendix A). Assuming that the frequency ramps applied to the Raman lasers are perfectly equal for the three Raman light pulses and that the laser intensities are the same for the first and last laser pulse, its contribution vanishes in the interferometer phase. However, technical imperfections lead to a bias phase proportional to β. We thus measured the acceleration as a function of the frequency chirp β. Figure 9 displays the acceleration signal measured by the hybridized atom accelerometer as a function of the chirp β. Each data point is obtained after an averaging time $\tau = 500$ s. The data are linear fitted, and no significant slope is obtained. From the fit uncertainty on the slope, one can estimate a maximum bias of $4.6 \times 10^{-5}\ \mathrm{m\,s^{-2}}$ for a frequency chirp $\beta = -210\ \mathrm{MHz}\ \mu\mathrm{s}^{-1}$.

IV. CONCLUSION

We have presented here an experimental demonstration of a method to address a single counterpropagating Raman transition in a retroreflected configuration despite zero Doppler shift. Using this method we have achieved a horizontal acceleration sensitivity of $3.2 \times 10^{-5}\ \mathrm{m\,s^{-2}}/\sqrt{\mathrm{Hz}}$ with a falling distance of 5.9 mm, which is competitive with state of the art [38]. Improving the atom accelerometer sensitivity could be simply achieved by using a larger laser beam radius combined with higher optical power, and a faster cycling rate. We have shown that the acceleration bias introduced by this method was constrained at the level $4 \times 10^{-5}\ \mathrm{m\,s^{-2}}$, even though modulating the laser diode current for frequency chirp is not the optimal way to achieve the best level of reproducibility. Thus, further work would be required to assess both long-term stability of the atomic sensor and absence of bias introduced by the frequency ramp. This method can easily be extended to other AI configurations involving four or more pulses [39,40], such as, for example, in a double-loop geometry with pulse sequence $(\pi/2 - \pi - \pi - \pi/2)$ for rotation measurements independent of acceleration [12]. Finally,this method appears suited for multiaxis inertial sensing using cold atoms without a need for tilted laser beams [41–43], as well as for compact tiltmeters or for experiments in microgravity environments using atom interferometers based on a single-diffraction process [44,45].

ACKNOWLEDGMENTS

We thank F. Nez from Laboratoire Kastler Brossel (LKB) for helpful discussions. M.C. acknowledges funding from ONERA through research project CHAMO (Central Hybride AtoMique de l'Onera).

APPENDIX A: FREQUENCY-CHIRP-INDUCED BIAS

1. Origin of the bias phase

In this Appendix we investigate the effect of chirping the Raman laser during the light pulses of the Mach-Zehnder atom interferometer. To calculate this effect, we express the interferometer phase shift as

$$\Delta\Phi = \phi_1 - 2\phi_2 + \phi_3, \tag{A1}$$

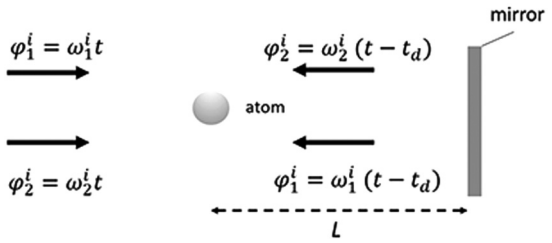

FIG. 10. Scheme of the cold atom interferometer. The resonant counterpropagating beams are obtained by retroreflecting the lasers on the mirror. Due to the retroreflection delay, if the Raman frequency is not perfectly the same at each Raman pulse, a bias phase arises.

where $\phi_i = \varphi_1^i - \varphi_2^i$ is the phase difference imprinted onto the atoms by the two counterpropagating Raman beams of frequencies ω_1 and ω_2 at the ith Raman pulse. Figure 10 is a schematic describing the interaction between atoms and Raman pulses. Considering the retroreflection delay $t_d = 2L/c$, where L is the distance from the atoms to the mirror, one finds the laser phase difference imprinted onto the atoms at the ith pulse is (see Fig. 10)

$$\phi_i(t) = \varphi_1(t) - \varphi_2(t - t_d) \tag{A2}$$

$$= \omega_1^{(i)} t - \omega_2^{(i)}(t - t_d), \tag{A3}$$

where $\omega_{1,2}^{(i)}$ is the Raman frequency at the ith laser pulse. Therefore, it turns out that if the Raman laser frequency is not perfectly the same for the three Raman laser pulses, it leads to a bias phase [4]:

$$\Delta\varphi_{\mathrm{bias}} = \left(\omega_1^{(1)} + \omega_1^{(3)} - 2\omega_1^{(2)}\right) \times t_d. \tag{A4}$$

Thus, in our experiment the reproducibility of the Raman laser frequency chirp within the interferometer interrogation time is crucial.

2. Calculations

To compute the bias phase induced by the frequency chirp on the Raman laser, we use the response function formalism. Thus, one can write the bias phase for the Mach-Zehnder type AI of Sec. III as

$$\Delta\varphi_{\mathrm{bias}} = \int_{-T-\frac{3\tau}{2}}^{T+\frac{3\tau}{2}} \phi_i(t) f^{(i)}(t)\, dt, \tag{A5}$$

where $f^{(i)}(t)$ is the response function of the atom interferometer at the ith pulse given by

$$f(t) = \begin{cases} \frac{\Omega_1 \cos[\Omega_1(t+T+\frac{3\tau}{2})]}{\sin(\Omega_1\tau)} & t \in \left[-T-\frac{3\tau}{2}, -T-\frac{\tau}{2}\right] \\ -\frac{\Omega_2 \cos(\Omega_2 t)}{\sin(\Omega_2\tau/2)}\ t \in \left[\frac{-\tau}{2}, \frac{\tau}{2}\right] & \\ \frac{\Omega_3 \cos[\Omega_1(t-T-3\tau/2)]}{\sin(\Omega_3\tau)} & t \in \left[T+\frac{\tau}{2}, T+\frac{3\tau}{2}\right] \\ 0 & \text{otherwise} \end{cases}, \tag{A6}$$

where Ω_i is the Rabi frequency of the ith laser pulse. The response function is displayed in Fig. 11 considering ($\Omega_1 = \Omega_3$ and $\Omega_2 = 2\Omega_1$). For the calculations, we consider the possibility of both a frequency offset change $\delta\omega_1$ of the

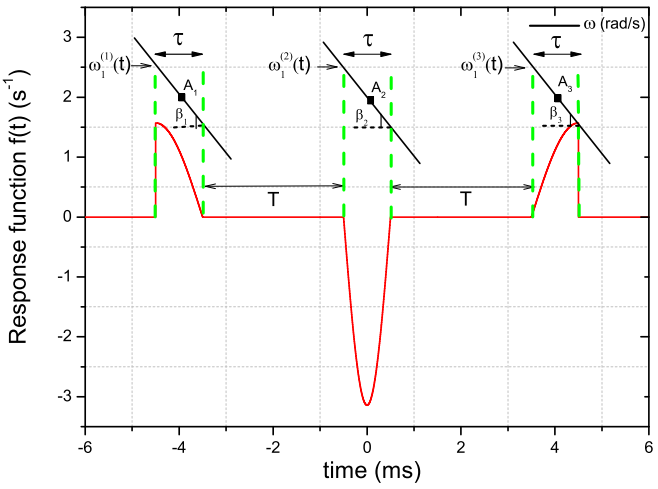

FIG. 11. Response function (in red) of the Mach-Zehnder AI for equal pulses of duration τ and considering that the π pulse occurs at $t = 0$. Here $T = 3$ ms and $\tau = 1$ ms for the sake of clarity. The intensity of the laser is the same for the first and last laser pulse (e.g., $\Omega_1 = \Omega_3$, $\Omega_2 = 2\Omega_{1,3}$). The green dashed line symbolizes the Raman pulse, and the black line represents the Raman frequency ramp characterized with parameters $\omega_1^{(i)}, A_i, \beta_i$.

Raman laser and a change in slope β of the frequency ramp from pulse to pulse. These effects are illustrated in Fig. 11. After some algebra, the laser phase at the ith Raman pulse can be written

$$\phi_i = A_i + 2\pi\beta_i t_d(t - t_i), \tag{A7}$$

where β_i is the frequency chirp slope at the ith Raman pulse, t_i, the time at the middle of the Raman pulse, and with

$$A_i = \left(\omega_1 + \delta\omega_1^{(i)}\right)t_d, \tag{A8}$$

where $\delta\omega_1^{(i)}$ is the laser frequency offset at the ith Raman pulse. The bias phase is obtained by analytically computing Eq. (A5), which leads to

$$\Delta\varphi_{\text{bias}} = A_1 - 2A_2 + A_3 + 2\pi t_d\frac{\tau}{2}(\beta_3 - \beta_1) + 2\pi t_d\left(\beta_3\frac{\cos(\Omega_3\tau) - 1}{\Omega_1\sin(\Omega_3\tau)} - \beta_1\frac{\cos(\Omega_1\tau) - 1}{\Omega_1\sin(\Omega_1\tau)}\right). \tag{A9}$$

The bias phase comprises three contributions. The first one corresponds to a change in the frequency offset of the ramp, the second one arises from a change of the chirp slope, and finally, the last contribution is a combination of the chirp slope variation and intensity change between the first and the last Raman laser pulse. This result confirms that for perfectly reproducible frequency ramps and assuming equal laser intensities ($\Omega_1 = \Omega_3$), the bias phase vanishes. However, experimental imperfections lead to a measurement bias. In order to derive realistic constraints on our experimental parameters, one can approximate Eq. (A9) to the first order in $\Delta\Omega/\Omega_1$ and $\Delta\beta/\beta$ (e.g., $\Omega\tau \sim \pi/2$). The following equation results:

$$\Delta\varphi_{\text{bias}} \simeq A_1 - 2A_2 + A_3 + 2\pi\Delta\beta t_d\tau\left(\frac{1}{2} - \frac{2}{\pi}\right) + 2\pi\beta t_d\tau\left(\frac{2}{\pi} - 1\right)\frac{\Delta\Omega}{\Omega_1}, \tag{A10}$$

where $\Delta\beta = \beta_3 - \beta_1$ and $\Delta\Omega = \Omega_3 - \Omega_1$. In our experimental scheme, one can assume that A_i and $\Delta\beta$ are proportional to β, leading to an overall bias phase proportional to β. Thus, measuring the acceleration as a function of the frequency chirp allows us to confine our experimental parameters. A measured acceleration bias at the level of 4×10^{-5} m s^{-2} requires a control of the experimental parameters at the level of $\delta\omega_1 \approx 2\pi \times 10$ MHz, $\frac{\Delta\beta}{\beta} \approx 10^{-2}$, and $\frac{\Delta\Omega}{\Omega_1} \approx 2 \times 10^{-2}$, respectively. Finally, increasing the sensitivity would require the reproducibility of the frequency ramp to be checked with a much higher precision, which was out of the scope of this work.

[1] A. Peters, K. Y. Chung, and S. Chu, Metrologia **38**, 25 (2001).
[2] P. Gillot, O. Francis, A. Landragin, F. Pereira Dos Santos, and S. Merlet, Metrologia **51**, 15 (2014).
[3] Z. K. Hu, B. L. Sun, X. C. Duan, M. K. Zhou, L. L. Chen, S. Zhan, Q. Z. Zhang, and J. Luo, Phys. Rev. A **88**, 043610 (2013).
[4] Y. Bidel, N. Zahzam, C. Blanchard, A. Bonnin, M. Cadoret, A. Bresson, D. Rouxel, and M.-F. Lequentrec-Lalancette, Nat. Commun. **9**, 627 (2018).
[5] M. Hauth, C. Freier, V. Schkolnik, A. Senger, M. Schmidt, and A. Peters, Appl. Phys. B **113**, 49 (2013).
[6] J. M. McGuirk, G. T. Foster, J. B. Fixler, M. J. Snadden, and M. A. Kasevich, Phys. Rev. A **65**, 033608 (2002).
[7] F. Sorrentino, Q. Bodart, L. Cacciapuoti, Y.-H. Lien, M. Prevedelli, G. Rosi, L. Salvi, and G. M. Tino, Phys. Rev. A **89**, 023607 (2014).
[8] X.-C. Duan, M.-K. Zhou, D.-K. Mao, H.-B. Yao, X.-B. Deng, J. Luo, and Z.-K. Hu, Phys. Rev. A **90**, 023617 (2014).
[9] T. L. Gustavson, P. Bouyer, and M. A. Kasevich, Phys. Rev. Lett. **78**, 2046 (1997).
[10] A. Gauguet, B. Canuel, T. Lévèque, W. Chaibi, and A. Landragin, Phys. Rev. A **80**, 063604 (2009).
[11] G. Tackmann, P. Berg, C. Schubert, S. Abend, M. Gilowski, W. Ertmer, and E. M. Rasel, New J. Phys. **14**, 015002 (2012).
[12] I. Dutta, D. Savoie, B. Fang, B. Venon, C. L. Garrido Alzar, R. Geiger, and A. Landragin, Phys. Rev. Lett. **116**, 183003 (2016).
[13] C. Jekeli, Navigation **52**, 1 (2005).
[14] R. H. Parker, C. Yu, W. Zhong, B. Estey, and H. Müller, Science **360**, 191 (2018).
[15] J. B. Fixler, G. T. Foster, J. M. McGuirk, and M. A. Kasevich, Science **315**, 74 (2007).
[16] R. Bouchendira, P. Cladé, S. Guellati-Khélifa, F. Nez, and F. Biraben, Phys. Rev. Lett. **106**, 080801 (2011).
[17] G. Rosi, F. Sorrentino, L. Cacciapuoti, M. Prevedelli, and G. M. Tino, Nature (London) **510**, 518 (2014).
[18] S. Fray, C. A. Diez, T. W. Hänsch, and M. Weitz, Phys. Rev. Lett. **93**, 240404 (2004).
[19] A. Bonnin, N. Zahzam, Y. Bidel, and A. Bresson, Phys. Rev. A **88**, 043615 (2013).

[20] D. Schlippert, J. Hartwig, H. Albers, L. L. Richardson, C. Schubert, A. Roura, W. P. Schleich, W. Ertmer, and E. M. Rasel, Phys. Rev. Lett. **112**, 203002 (2014).
[21] M. G. Tarallo, T. Mazzoni, N. Poli, D. V. Sutyrin, X. Zhang, and G. M. Tino, Phys. Rev. Lett. **113**, 023005 (2014).
[22] L. Zhou, S. Long, B. Tang, X. Chen, F. Gao, W. Peng, W. Duan, J. Zhong, Z. Xiong, J. Wang, Y. Zhang, and M. Zhan, Phys. Rev. Lett. **115**, 013004 (2015).
[23] P. Hamilton, M. Jaffe, P. Haslinger, Q. Simmons, H. Müller, and J. Khoury, Science **349**, 849 (2015).
[24] S. Dimopoulos, P. W. Graham, J. M. Hogan, M. A. Kasevich, and S. Rajendran, Phys. Rev. D **78**, 122002 (2008).
[25] W. Chaibi, R. Geiger, B. Canuel, A. Bertoldi, A. Landragin, and P. Bouyer, Phys. Rev. D **93**, 021101(R) (2016).
[26] P. Hamilton, A. Zhmoginov, F. Robicheaux, J. Fajans, J. S. Wurtele, and H. Müller, Phys. Rev. Lett. **112**, 121102 (2014).
[27] M. Kasevich and S. Chu, Phys. Rev. Lett. **67**, 181 (1991).
[28] V. Schkolnik, B. Leykauf, M. Hauth, C. Freier, and A. Peters, Appl. Phys. B **120**, 311 (2015).
[29] D. S. Durfee, Y. K. Shaham, and M. A. Kasevich, Phys. Rev. Lett. **97**, 240801 (2006).
[30] T. Lévèque, A. Gauguet, F. Michaud, F. Pereira Dos Santos, and A. Landragin, Phys. Rev. Lett. **103**, 080405 (2009).
[31] N. Malossi, Q. Bodart, S. Merlet, T. Lévèque, A. Landragin, and F. Pereira Dos Santos, Phys. Rev. A **81**, 013617 (2010).
[32] O. Carraz, C. Siemes, L. Massotti, R. Haagmans, and P. Silvestrin, Microgravity Sci. Technol. **26**, 139 (2014).
[33] I. Perrin, Y. Bidel, N. Zahzam, C. Blanchard, A. Bresson, and M. Cadoret, Phys. Rev. A **99**, 013601 (2019).
[34] F. Théron, Y. Bidel, E. Dieu, N. Zahzam, M. Cadoret, and A. Bresson, Opt. Commun. **393**, 152 (2017).
[35] F. Théron, O. Carraz, G. Renon, N. Zahzam, Y. Bidel, M. Cadoret, and A. Bresson, Appl. Phys. B **118**, 1 (2015).
[36] O. Carraz, R. Charrière, M. Cadoret, N. Zahzam, Y. Bidel, and A. Bresson, Phys. Rev. A **86**, 033605 (2012).
[37] J. Lautier, L. Volodimer, T. Hardin, S. Merlet, M. Lours, F. P. D. Santos, and A. Landragin, Appl. Phys. Lett. **105**, 144102 (2014).
[38] W.-J. Xu, M.-K. Zhou, M.-M. Zhao, K. Zhang, and Z.-K. Hu, Phys. Rev. A **96**, 063606 (2017).
[39] B. Dubetsky and M. A. Kasevich, Phys. Rev. A **74**, 023615 (2006).
[40] M. Cadoret, N. Zahzam, Y. Bidel, C. Diboune, A. Bonnin, F. Théron, and A. Bresson, J. Opt. Soc. Am. B **33**, 1777 (2016).
[41] B. Canuel, F. Leduc, D. Holleville, A. Gauguet, J. Fils, A. Virdis, A. Clairon, N. Dimarcq, C. J. Bordé, A. Landragin, and P. Bouyer, Phys. Rev. Lett. **97**, 010402 (2006).
[42] Y.-J. Chen, A. Hansen, G. W. Hoth, E. Ivanov, B. Pelle, J. Kitching, and E. A. Donley, Phys. Rev. Appl. **12**, 014019 (2019).
[43] X. Wu, F. Zi, J. Dudley, R. J. Bilotta, P. Canoza, and H. Müller, Optica **4**, 1545 (2017).
[44] R. Geiger, V. Ménoret, G. Stern, N. Zahzam, P. Cheinet, B. Battelier, A. Villing, F. Moron, M. Lours, Y. Bidel, A. Bresson, A. Landragin, and P. Bouyer, Nat. Commun. **2**, 474 (2011).
[45] B. Barrett, L. Antoni-Micollier, L. Chichet, B. Battelier, T. Lévèque, A. Landragin, and P. Bouyer, Nat. Commun. **7**, 13786 (2016).